

MC3D - 3D Continuum Radiative Transfer Version 2

S. Wolf^a

^a*California Institute of Technology, 1200 E California Blvd, Mail Code 220-6,
Pasadena CA 91125, USA, swolf@ipac.caltech.edu*

Abstract

A revised and greatly improved version of the 3D continuum radiative transfer code MC3D is presented. It is based on the Monte-Carlo method and solves the radiative transfer problem self-consistently. It is designed for the simulation of dust temperatures in arbitrary geometric configurations and the resulting observables: spectral energy distributions, wavelength-dependent images, and polarization maps. The main objective is the investigation of “dust-dominated” astrophysical systems such as young stellar objects surrounded by an optically thick circumstellar disk and an optically thin(ner) envelope, debris disks around more evolved stars, asymptotic giant branch stars, the dust component of the interstellar medium, and active galactic nuclei.

PACS: 95.30.Jx – Radiative transfer

Key words: Continuum radiative transfer; Monte-Carlo method; Numerical simulation; Polarization; Circumstellar shells

1 Introduction

The 3D continuum radiative transfer (RT) code, MC3D, combines the most recent Monte Carlo (MC) radiative transfer concepts for both the self-consistent RT, i.e., the estimation of spatial dust temperature distributions, and pure scattering applications, taking into account the polarization state of the radiation field. It has been tested intensively and compared with grid-based and MC RT codes (see, e.g., Pascucci et al. (1), Wolf (2)).

In addition to the previous version of MC3D (Wolf & Henning (3); see also Wolf et al. (4)), MC3D (V2) contains several improvements which allow a much more efficient solution of the radiative transfer problem in three-dimensional, arbitrary dust configurations. The main features are:

- A new concept for *estimation of dust temperature distributions* which was first described by Bjorkman & Wood (5) in the context of the solution of the radiative transfer problem in circumstellar disks. It is based on the immediate correction of the dust grain temperature and the reemission radiation field after absorption of a photon packet. Beyond a faster estimation of the dust equilibrium temperature without iterations, it allows the application of the code for optical depths far above the previous $\tau \approx 10^3$ limit.
- A new concept for the *test photon transfer*, based on the work of Lucy (6), (previously developed for one-dimensional model geometries), which takes into account the absorption not only at the points of interaction of the test photons with the dust grains but also in between. Therefore, the temperature correction can be performed in all volume elements on the test photon path and consequently, there is no more lower optical depth limit for the application of MC3D.
- A new concept for the simulation of scattering in optically thin dust/electron configurations which has been firstly described by Cashwell & Everett (7) (see also Witt (8) and Ménard (9) for former applications in one- and two-dimensional model geometries) which makes use of the *enforced scattering method*.
- The simulation of the RT in *dust grain mixtures* consisting of grains with different chemical composition and size.
- A *raytracer* for the simulation of images and spectral energy distributions (SEDs) which may be used for the simulation of the dust reemission in the midinfrared-millimeter wavelength range, where scattering is of minor importance.
- An accelerated solution of the temperature estimation in flat disks with or without vertical density structure.

These features have been adapted to and tested for several 1D, 2D, and 3D model geometries which are shown in Fig. 1.

Previous applications of MC3D cover feasibility studies of extrasolar planet detections (Wolf et al. (10)), the RT in the clumpy circumstellar environment of young stellar objects (Wolf et al. (11)), polarization studies of T Tauri stars (Wolf et al. (12)), AGN polarization models (Wolf & Henning (13)), a solution for the multiple scattering of polarized radiation by non-spherical grains (Wolf et al. (14)), and the inverse RT based on the MC method (Wolf (15)).

The executables of MC3D (V2) can be downloaded for several model geometries and computer platforms from

<http://www.mpia-hd.mpg.de/FRINGE/SOFTWARE/mc3d/>

(current US mirror page:

<http://spider.ipac.caltech.edu/staff/swolf/mc3d/>).

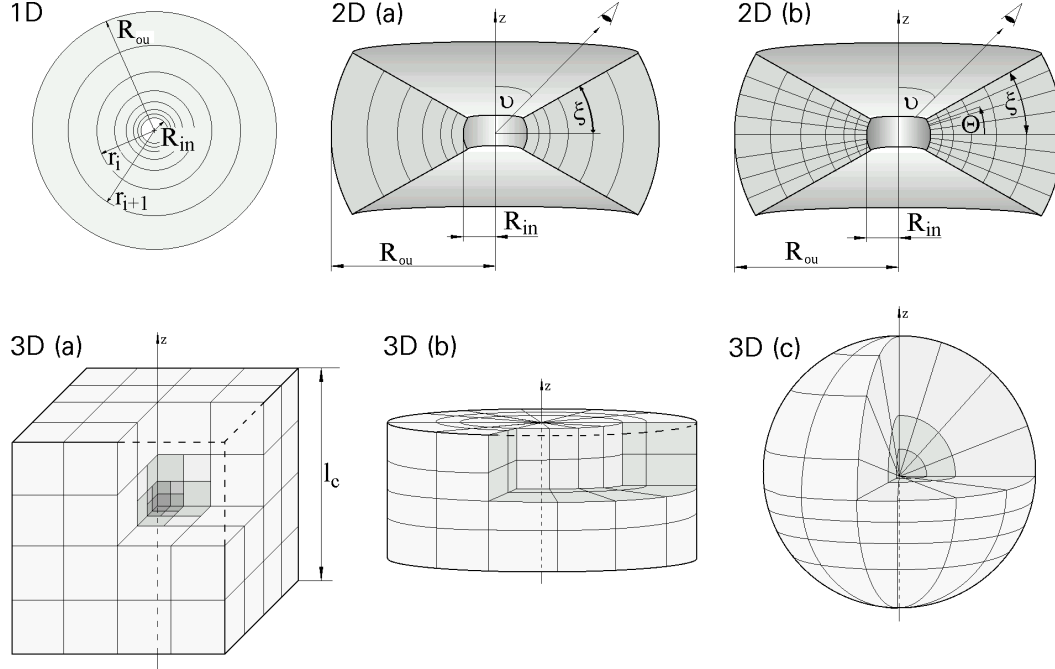


Fig. 1. Model geometries: Examples for the subdivision of the model space into energy storage cells (see Sect. 3.3 for further explanations). **1D**: radial symmetry; **2D(a)**: radial symmetry inside a disk; **2D(b)**: fully two-dimensional model for configurations with a radial and vertical dependence of the density distribution; **3D(a-c)**: three-dimensional models considered in cartesian, cylindrical, and spherical coordinates.

Furthermore, a detailed description, usage instructions, and IDL¹ routines for a subsequent data analysis of the code are provided there. Very frequently used model geometries, such as disks with a radial and vertical variable density distribution, which is often used for the analysis of SEDs, images and polarization maps of circumstellar disks (see, e.g., Wood et al. (16), Cotera et al. (17), Fischer et al. (18)), are available. However, the author encourages the reader to ask for further model geometries.

In Sect. 2 the general scheme for the solution of the RT problem on the basis of the MC method as it is applied in MC3D is briefly outlined. In Sect. 3 the two different concepts for the estimation of the spatial dust temperature distribution (iterative radiative transfer and immediate reemission) are discussed. In the following Sect. 4, the determination of the observables is described, and Sect. 5 introduces further concepts which are used in MC3D in order to increase the efficiency of the RT algorithms.

¹ Interactive Data Language

2 General remarks about the applied solution of the radiative transfer problem

Each model to be considered with MC3D consists of two independently defined components:

- (1) The spatial density distribution of the scattering and absorbing medium, and
- (2) The radiative source(s).

Both must be defined inside a convex model space in order to exclude the case of radiation leaving the model space at one point and entering it at another.

2.1 *Scattering and absorbing medium*

MC3D handles spherically symmetric scatterers/absorbers, such as spherical dust grains and electrons (in the Thomson scattering regime). The required optical properties, i.e., the absorption and extinction efficiency (Q_{abs} , Q_{ext}), the special Mueller matrix \hat{S} (see Sect. 2.3, App. C), and quantities to be derived from these – the albedo A , the extinction and scattering cross section (C_{ext} , Q_{sca}), and the scattering function – can be calculated with an embedded Mie scattering routine (using the Mie scattering algorithm published by Bohren & Huffman (19)) on the basis of the real and imaginary refractive index (n, k) and the particle radius a . Since Thomson scattering can be – formally – considered as a special form of the Mie scattering formalism (no absorption, no wavelength dependence), in the following only dust grains are considered as the scattering and absorbing medium, covering also the special case of electrons.

MC3D allows simulation of the RT in arbitrary density distributions $\rho_j(\vec{r})$, where \vec{r} represents the spatial coordinate and the index j refers to the considered dust species (characterized by the grain size and chemical composition). If MC3D is used to simulate the *scattering* by dust grains only (for instance for the simulation of images, polarization maps or SEDs in the visual-midinfrared wavelength range), the mean optical properties of dust grain mixtures consisting of 3 chemically different components and a size distribution following a power-law $n(a) \propto a^{-\alpha}$ ($n(a)$ is the number of dust grains with the radius a ; $\alpha = \text{const.}$) can be estimated on the basis of the formalism being described in Appendix A. As found by Wolf (20), this concept of mean dust grains also represents a reasonable approximation for the estimation of temperature distributions in optically thick density distributions and the simulation of SEDs in general.

The density distribution may be defined either analytically or on a predefined grid in order to allow the implementation of density distributions resulting from hydrodynamical simulations (for examples, see Wolf et al. (4), Sect. 4; Wolf et al. (10)).

2.2 Radiation sources

In principle, radiation sources, that are arbitrary with respect to their number and spatial configuration, spatial extent, intrinsic SED, and radiation characteristic can be considered (see Wolf et al. (4), (10) for examples). In MC3D the RT is simulated at certain wavelengths within the wavelength range $[\lambda_{\min}, \lambda_{\max}]$. For this reason, the monochromatic luminosity² L_λ of the radiation source(s) is partitioned into n_{Photon} so-called “weighted photons” (Sobolev (21)) each of which is characterized by its wavelength λ and Stokes vector $\hat{I} = (I, Q, U, V)^T$. The polarization state of a photon is determined by the Stokes vector components as follows:

$$\begin{aligned} \text{(a) Linear polarization degree} & : P_l = \frac{\sqrt{(Q^2+U^2)}}{I} \\ \text{(b) Orientation of the linear polarization} & : \gamma = \frac{1}{2} \arctan\left(\frac{U}{Q}\right) \\ \text{(c) Circular polarization degree} & : P_c = \frac{V}{I} \end{aligned} \quad (1)$$

The two main radiation sources in MC3D RT simulations shall be introduced in brief:

- (1) Pointlike Star: Here the emission direction of photons, described in spherical coordinates (θ_E, ϕ_E) is given by

$$\cos \theta_E = -1 + 2 Z_1, \quad \phi_E = 2 \pi Z_2, \quad (2)$$

- (2) Extended Star (radius R_s , radiation characteristic at each point on the stellar surface: $I \propto \cos(\theta'_E)$):

$$\sin \theta'_E = \sqrt{Z_3}, \quad \phi'_E = 2 \pi Z_4, \quad (3)$$

whereby θ'_E and ϕ'_E are related to the z' axis parallel to the radius vector (R_s, θ_E, ϕ_E) which can be determined using Eq. 2 (see Fig. 2 for explanation). Here and in the following, Z_i ($i = 1, 2, \dots$) are random numbers uniformly distributed in the interval $[0, 1]$. For their determination a random number generator, which minimizes the sequential correlations between random numbers by the combination of different random number generators, is

² Between the (bolometric) luminosity L and the monochromatic luminosity L_λ the following relation exists: $L = \int_0^\infty L_\lambda d\lambda$.

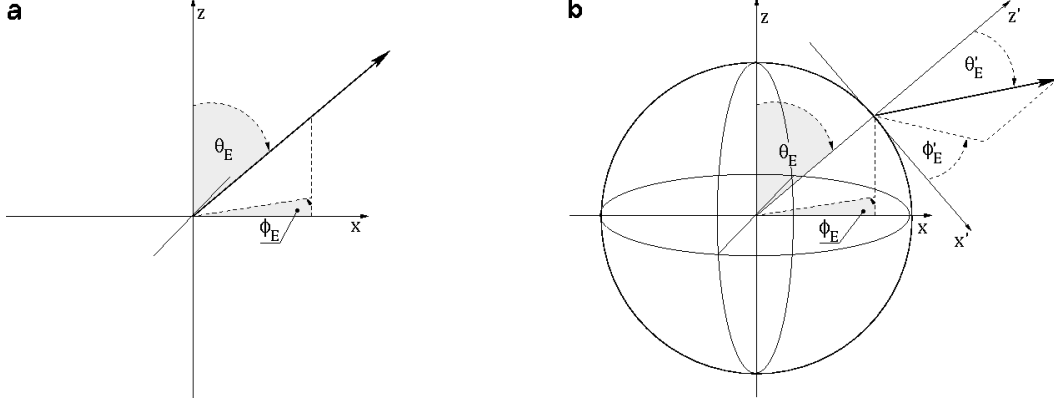


Fig. 2. Emission angles. [a] Pointlike star, [b] Extended source.

used (Knuth (22)). The Stokes vector of a newly emitted, unpolarized photon is defined as $\vec{I}_0 = (I, Q, U, V)_0^T = (1, 0, 0, 0)^T$.

Assuming the dust grains to be spherical, the direction of photon reemission can be determined as for point-like stars shown in Fig. 2[A] (Eq. 2). Since the point of reemission inside certain volume elements of the model space (energy storage cells, ESCs - see Sect. 3.3) is assumed to be constant, the location of the reemitting dust grains has to be chosen randomly therein, assuming a constant density distribution within the cell. The determination of the point of reemission within an ESC is described for the different model geometries shown in Fig. 1 in App. D.

2.3 Photon transfer and scattering

The mean free path length l between the point of emission and the point of the first photon-dust interaction (and - subsequently - between two points of interaction) is given by (see App. B)

$$\tau_{\text{ext},l} = -\ln(1 - Z_5), \quad (4)$$

$$\tilde{\tau}_{\text{ext},l} = \sum_{i=1}^{i_{\text{end}}} \left[\sum_{j=1}^{n_D} \rho_j(\vec{r}_{l_i}) \cdot C_{\text{ext}j} \right] \cdot \Delta l_i, \quad l = \sum_{i=1}^{i_{\text{end}}} \Delta l_i. \quad (5)$$

Here, n_D is the number of different dust grain species and \vec{r}_{l_i} is the spatial coordinate corresponding to the i th integration point along the path length l .

The step width Δl_i has to be small enough to satisfy the linear approximation of the extinction cross section and density distribution along the path of the photon (Eq. 5). The step width Δl_i is not fixed but has an initial (maximum) value which is chosen to be a fraction of the extent of the current energy storage

cell (ESC, see Sect. 3.3 for an introduction to the ESC concept) the photon is moving through – or, if any of the neighboring cells is smaller, then of that. This procedure ensures that no ESC is skipped on the photon’s path. Because the subdivision into ESCs is adapted to the model geometry and distribution of the local optical depth, this coupling drastically increases the efficiency of the photon transfer since a small step width in high density regions as well as large step widths in low density (gradient) regions is provided simultaneously. In order to minimize the difference between the exact value $\tau_{\text{ext},1}$ and the numerically achieved value $\tilde{\tau}_{\text{ext},1}$, Δl_i is decreasing as soon as the test photon reaches the vicinity of the next interaction point.

This photon transfer concept was found to limit the applicability of previous version of MC3D to optical depths $\tau \geq 10^{-3}$ (Wolf & Henning (3)) since the probability for photons to interact with the (circumstellar) matter is negligibly small for even lower optical depths (it decreases exponentially as described by Bouguer-Lambert’s law). In order to be able to consider lower optical depths, for instance the simulation of the scattered light arising from an optically thin envelope or the electron environment around hot stars, the concept of enforced scattering (Cashwell & Everett (7)) has been implemented. The idea is to force each photon to be scattered at least once between the point of emission and the boundary of the model space, provided there is dust on its path (optical depth $\tau_{\text{ext}0}$). A fraction of the photon ($e^{-\tau_{\text{ext}0}}$) leaves the model space without interaction while the remaining part ($1 - e^{-\tau_{\text{ext}0}}$) will be scattered. Following the same strategy as for the determination of the mean path length (see App. B), we derive:

$$f(\tau_{\text{ext}})d\tau_{\text{ext}} = \frac{I_0 \cdot e^{-\tau_{\text{ext}}} \cdot d\tau_{\text{ext}}}{\int_0^{\tau_{\text{ext}0}} I_0 \cdot e^{-\tau_{\text{ext}}} d\tau_{\text{ext}}} = \frac{e^{-\tau_{\text{ext}}} \cdot d\tau_{\text{ext}}}{1 - e^{-\tau_{\text{ext}0}}} \quad (6)$$

$$Z = F(\tau_{\text{ext}}) = \int_0^{\tau_{\text{ext}}} f(\tau'_{\text{ext}}) d\tau'_{\text{ext}} = \frac{1 - e^{-\tau_{\text{ext}}}}{1 - e^{-\tau_{\text{ext}0}}} \quad (7)$$

$$\tau_{\text{ext}} = -\ln(1 - Z[1 - e^{-\tau_{\text{ext}0}}]). \quad (8)$$

As Fig. 3 illustrates, the enforced scattering concept is of tremendous importance for the simulation of scattered light of, e.g., the optically thin envelope of young stellar objects, debris disks around more evolved stellar systems, or the zodiacal light in extra-solar planetary systems.

Depending on the applied concept for the temperature estimation (see Sect. 3), scattering or absorption or both processes occur at a point of interaction. The modification of the Stokes vector due to the i th scattering is described by a special Müller matrix $\hat{S}_j(\theta, \phi)$ of the dust grain species number j (see, e.g.,

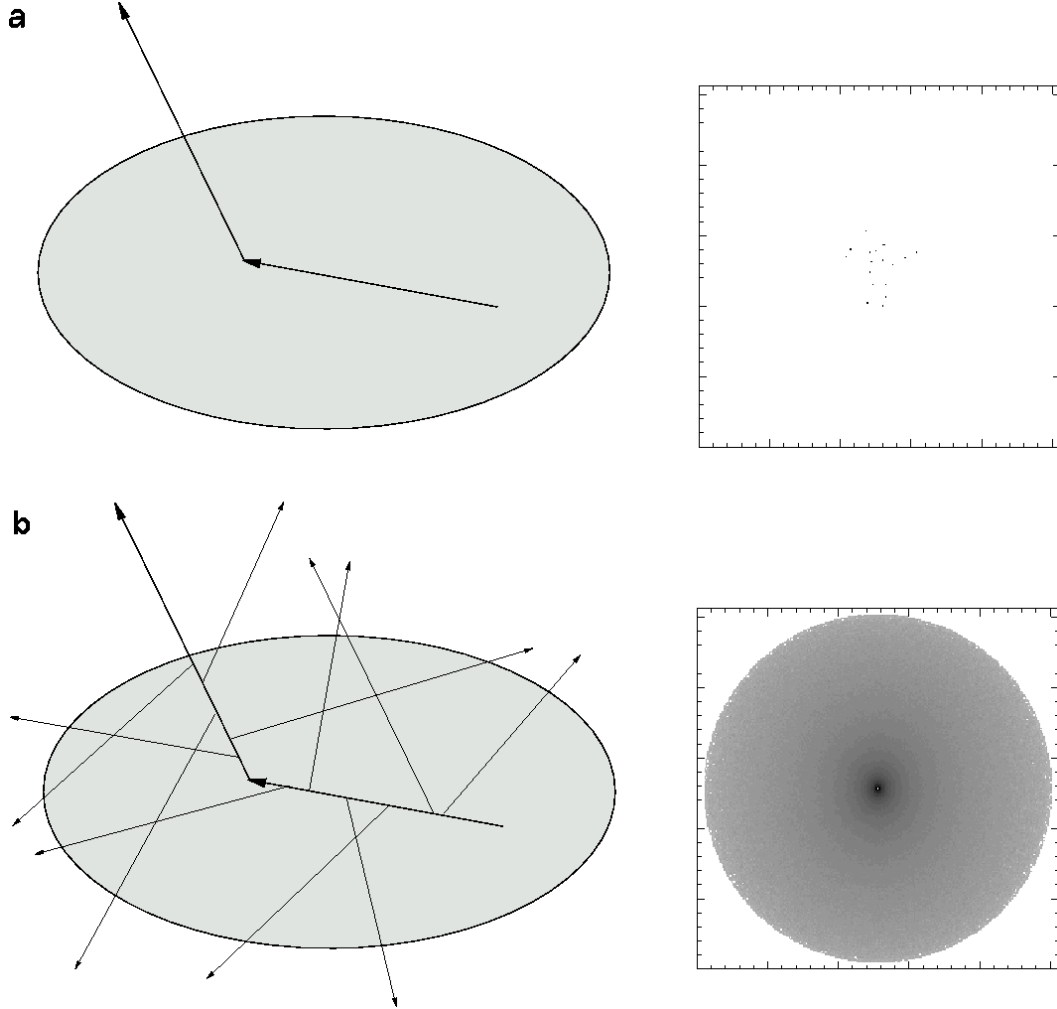


Fig. 3. Illustration of the high efficiency of the enforced scattering concept in optically very thin configurations. (a) Without and (b) with enforced scattering. Spherical shell being illuminated by an embedded star. Density profile: $\rho(r) \propto r^{-0.5}$. Optical depth at the considered wavelength (as seen from the star): 10^{-6} . Number of photons: 10^7 . Shown is the $(\text{Intensity})^{1/8}$ without the central star. The required CPU time amounts in both cases to about 7 min (using a Intel Celeron, 1.2GHz processor).

Bickel & Bailey (23), Bohren & Huffman (19)):

$$\hat{I}_i \propto \hat{S}_j(\theta, \phi) \hat{I}_{i-1} . \quad (9)$$

Here, θ and ϕ are the scattering angles (see App. C). The estimation of the scattering direction, based on the scattering function provided by Mie calculations, and the consideration of multiple scattering events, taking into account (the change of) the polarization state of the weighted photon, are based on the concepts described by Fischer et al. (24), App. A 3 and A 4.2. The absorption and reemission processes are described in the context of the temperature

estimation in Sect. 3.

3 Estimation of the spatial temperature distribution

Two different concepts for the solution of the self-consistent RT problem, i.e., the determination of the spatial dust temperature distribution on the basis of the amount of absorbed energy of the stellar and the dust reemission radiation field, are embedded in MC3D. While the first is based on an iterative procedure (Sect. 3.1), in the second the temperature distribution is changed (“updated”) simultaneously with each absorption act (Sect. 3.2).

3.1 Iterative Radiative Transfer

Assuming a star with an effective temperature T_{eff} and radius R_* , its monochromatic luminosity (assuming blackbody radiation) can be written as

$$L_{\lambda, \text{Stern}}^e = 4\pi R_*^2 \cdot \pi B_\lambda(T_{\text{eff}}), \quad (10)$$

where $B_\lambda(T)$ is the Planck function. Due to absorption of stellar and reemitted radiation the dust is heated. Absorption occurs simultaneously to the scattering whereby the probability for a dust grain of the species j to be the interaction partner of the photon is given by

$$\Pi_1(j) = \frac{\rho_j(\vec{r}) \cdot C_{\text{ext}_j}}{\sum_{j'=1}^{n_D} [\rho_{j'}(\vec{r}) \cdot C_{\text{ext}_{j'}}]} \quad (11)$$

The difference ΔI of the Stokes parameter I before and after the absorption process is determined by the wavelength-dependent albedo of the dust grains A_{λ_j} :

$$\Delta_i I = I_{i-1} \cdot (1 - A_{\lambda_j}). \quad (12)$$

Consequently, the amount of monochromatic luminosity represented by the particular photon is decreased by

$$\Delta_i L_\lambda = \frac{L_\lambda}{n_{\text{Photon}}(\lambda)} \cdot \Delta_i I. \quad (13)$$

The monochromatic luminosity of a single spherical dust grain with the radius a , the temperature T_g , and the wavelength-dependent absorption efficiency

Q^{abs} can be written as

$$L_{\lambda, \text{g}}^{\text{e}} = 4\pi a^2 \cdot Q_{\lambda_j}^{\text{abs}}(a) \cdot \pi B_{\lambda}(T_{\text{g}}). \quad (14)$$

Assuming a static dust configuration, the energy being reemitted by all grains of the dust species j within the volume element V during the time interval Δt has to be equal to the energy being absorbed by the grains (local energy conservation):

$$\Delta t \cdot N_{V_j} \int_0^{\infty} L_{\lambda_j}^{\text{e}} d\lambda = \Delta t \cdot \int_0^{\infty} L_{\lambda_{V_j}}^{\text{abs}} d\lambda, \quad (15)$$

where N_{V_j} is the number of dust grains (species j) in the volume V . The absorbed monochromatic luminosity $L_{\lambda_{j,V}}^{\text{abs}}$ within the volume V is the accumulated amount of absorbed photon “fractions”:

$$L_{\lambda_{j,V}}^{\text{abs}} = \sum_{k=1}^{n_{\text{Photon}}} \sum_{i=0}^{n_{\text{abs}}(j,k)} \left(\Delta_i L_{\lambda_j} \right)_k, \quad (16)$$

where $n_{\text{abs}}(j, k)$ is the number of absorption acts of the k th photon by the dust species j in the volume V . The combination of Eq. 14 and 15 results in an equation which allows determination of the mean dust grain temperature \bar{T}_{g_j} in the volume V :

$$\frac{\int_0^{\infty} L_{\lambda_{j,V}}^{\text{abs}} d\lambda}{N_V \cdot 4\pi a^2 \cdot \pi} = \int_0^{\infty} Q_{\lambda_j}^{\text{abs}}(a) \cdot B_{\lambda}(\bar{T}_{\text{g}_j}) d\lambda. \quad (17)$$

Since the temperature \bar{T}_{g_j} cannot be separated from Eq. 17, in MC3D it is determined from a table of precalculated values of the right-hand integral in the range of 0 K to the dust sublimation temperature. A temperature step width of 0.1 K was found to be sufficiently small for most astrophysical applications.

To consider both, the stellar heating and the subsequent dust reemission radiation, the following iterative procedure is applied:

- (1) Heating by the star.
- (2) Reemission by the dust grains, based on the energy being absorbed from the stellar radiation field. The determination of the reemission coordinates in the ESCs depends on the configuration and is described in App. D in detail.
- (3) Reemission of the dust grains, based on the sum of the energy being absorbed from the stellar and the dust reemission radiation field.

The third step has to be repeated as long as the difference between the input energy (given by the stellar radiation field) and the output energy (given by the sum of the attenuated stellar radiation field and the reemitted radiation outside the model space) is larger than a user-specific threshold (e.g., 0.1% of the input energy).

3.2 Immediate Reemission

The second concept embedded in MC3D for the estimation of the spatial dust temperature distribution has been developed by Bjorkman & Wood (5). In contrast to the iterative concept (Sect. 3.1), *either* scattering or absorption occurs at a point of interaction of a photon with a dust grain. The probability for a photon to undergo the one or the other interaction process is given by

$$\Pi_x(j, \vec{r}) = \frac{\rho_j(\vec{r}) \cdot C_{x_j}(\vec{r})}{\sum_{j'=1}^{n_D} [\rho_{j'}(\vec{r}) \cdot C_{ext_{j'}}(\vec{r})]}, \quad (18)$$

where 'x' stands for either absorption or scattering. When a photon packet is absorbed, the new dust temperature is calculated immediately based on Eq. 17. To correct the ESC temperature, the wavelength of the immediately reemitted photon is chosen so that it corrects the temperature of the spectrum previously emitted by this particular ESC, i.e., the probability distribution of the reemission wavelength is given by

$$f(\lambda) \propto Q_{\text{abs}} [B_\lambda(\bar{T}_{\text{g}_j}(i)) - B_\lambda(\bar{T}_{\text{g}_j}(i-1))], \quad (19)$$

where $\bar{T}_{\text{g}_j}(i-1)$ represents the temperature of the grain species j before and $\bar{T}_{\text{g}_j}(i)$ after the i th absorption process in the considered ESC. The value of the monochromatic luminosity of the reemitted photon results from the corresponding energy conservation equation:

$$L_{\lambda_1} d\lambda_1 = L_{\lambda_2} d\lambda_2, \quad (20)$$

where $d\lambda_1$ and $d\lambda_2$ are the wavelengths of the absorbed/reemitted photon. As the simulation runs, the temperature distribution (and the SED given by the photons leaving the model space – see Sect. 4) relaxes to its equilibrium value without iterations.

To reduce the number of photons being required for the temperature estimation in optically thin configurations, the concept of Lucy (6) is applied. It considers the absorption of the electromagnetic radiation field not only at the

end points of the photon path (points of interaction) but also in between. The absorption due to all dust grain species has to be taken into account:

$$\tau_{\text{abs}} = \sum_{j=1}^{n_D} \int_{\text{point}_1}^{\text{point}_2} C_{\text{abs}_j} \cdot \rho_j(\vec{r}) \, dr. \quad (21)$$

The example of a circumstellar disk with an optically thin envelope shown in Fig. 4 illustrates the great potential of this concept.

3.3 ESC concept

To achieve a spatially resolved dust temperature distribution, the model space is subdivided into so-called energy storage cells (ESC) in which the absorbed energy of the radiation field is stored (accumulated) and in which a constant dust temperature is assumed. To represent the spatial temperature structure according to the model geometry, defined by both the spatial distribution of radiation sources and the dust density, the model space has to be subdivided taking this into account. Furthermore, the spatial distribution of the optical depth has to be taken into account in order to resolve the high temperature gradient in optically thick regions. Finally, the size of the ESCs also has to decrease towards the radiation source even in case of optically thin configurations to trace the steep temperature gradient resulting from the geometrical dilution of the radiation field. Fortunately, the last two conditions are fulfilled simultaneously for most astrophysical applications since the density gradient increases towards the radiation source(s).

While the ESC distributions 1D, 2D(a), 2D(b), 3D(b), and 3D(c), shown in Fig. 1, are fully determined by user specific parameters (such as the number of ESCs and the refinement factors for the model space towards the central object and/or the disk midplane), model 3D(a) is prepared to provide an adaptive ESC generation according to the constraints described above. The model space described by model 3D(a) is a cube with the side length l_c . It is subdivided according to the distribution of the optical depth. Here, the quantity

$$\rho_V = \sum_{j=1}^{n_D} C_{\text{ext}}(j) \cdot \tilde{N}_V(j) \quad (22)$$

is defined, where $\tilde{N}_V(j)$ is the number of dust grains (species j) in the volume element V ($V \leq l_c^3$). At the first step, ρ_V is estimated inside the whole model space ($\rho_V = \rho_0$). In the second step, the model space is subdivided into 8

cubes (side length $l_c/2$). In each “sub-cube” the relation

$$\frac{\rho_V(b)}{\rho_0} \leq \Xi \leq 1 \quad (23)$$

is checked, whereby $\rho_V(b)$ is the value of ρ_V in the cube i_c and Ξ is a user-specific quantity which controls the subdivision depth (number of subdivision levels). In the subsequent steps all sub-cubes for which the relation (23) is not fulfilled, the subdivision is continued. Finally, the model space is subdivided into cubes with the side length $\left(\frac{1}{2}\right)^{i_c} l_c$ ($i_c = 1, 2, \dots$). To prevent this algorithm ending up with too large a number of cubes (large RAM requirement), resulting from a too small value given for Ξ , the maximum number of cubes is a second user-specific parameter (constraint) of this algorithm. If the number of cubes exceeds this value, Ξ is increased, the subdivision process starts again, and so on.

4 Observables

Polarization maps, images, and SEDs are the observables which can be directly simulated with MC3D. For this reason the RT transfer is simulated independently for both the star and the dust as the sources of emission. The RT is performed as described in Sect. 2.3 and Sect. 3.1, Eq. 10-14 but without iterations. Although the immediate reemission concept provides the SED and images as a direct result of the RT too (see Sect. 3.2), it is not discussed here since the polarization state of the radiation is not considered and a decoupling of the short-wavelength stellar radiation and the long-wavelength dust reemission (and the simultaneous decoupling of the radiation at separate wavelengths) provides more freedom for the selection of the considered wavelength (range) for which the observables shall be simulated. See also Sect. 5 for a description of the implemented raytracer which can be used to derive the dust reemission SED and images.

In order to derive the observables, a photon will be projected onto an observing plane oriented perpendicular to the path of the photon as soon as its next scattering position would be located outside the model space (see Fig. 5[A]). Consequently – in approximation of real observations – only those photons will be projected onto the same plane which leave the model space in parallel directions. The number of observing planes is – with regard to the possible last scattering direction – potentially infinite.

The next step is to combine all those observing maps to a single map for which the angular distance of their normal vector to a given direction is smaller

than the angle ω (see Fig. 5[B]). The sum of the monochromatic luminosity of all photons collected on this map therefore represents the monochromatic luminosity $L'_{\lambda,\Omega}$ ($L'_{\lambda,\Omega} \leq L'_\lambda$) of the object seen under the solid angle $\Omega_{[\text{sr}]} = 2\pi(1 - \cos \omega_{[\text{rad}]})$.

Let σ_A be the radiating area of an object seen in projection on the observing plane. Then, the corresponding monochromatic intensity I_λ of the object is

$$I_\lambda = \frac{L'_{\lambda,\Omega}}{\Omega \cdot \sigma_A} . \quad (24)$$

The flux density S_λ at the point of observation is determined by the distance d between the object and the observer as follows:

$$S_\lambda = \frac{\sigma_A}{d^2} \cdot I_\lambda . \quad (25)$$

In order to derive spatially resolved images (such as shown in Fig. 4), the observing planes are subdivided in pixels. Regarding the last scattering position of a photon, its (projected) Stokes parameters, wavelength and monochromatic luminosity are stored in the corresponding pixel. The required transformation of the Stokes vector was outlined by Fischer (25).

5 Diverse further embedded concepts

(1) Selective Emission (for self-consistent RT)

(a) *Wavelength range selection:*

The CPU time can be drastically reduced by considering only those wavelength ranges in which the particular radiative source (the star or the dust in a certain ESC) is emitting a non-negligible amount of energy (see Wolf & Henning 2000) for details.

(b) *Geometrical selection:*

For certain astrophysical models, the efficiency can be improved by excluding photons which would be emitted into dust free regions.

Example: *Circumstellar disk with a very small opening angle ξ (see Fig. 1, models 2D(a) and 2D(b)) around a pointlike star: Considering only those photons being emitted into the disk, the number of photons required to achieve a certain accuracy is reduced by a factor of $1/\sin \xi$. In contrast to Eq. 2, the angles of emission are now given by*

$$\cos \theta_E = (-1 + 2 Z_6) \cdot \sin(\xi), \quad \phi_E = 2 \pi Z_7. \quad (26)$$

- (2) Taking into account the symmetry of the considered model, the observing concept described in Sect. 4 can be modified in order to combine observing planes to a larger (effective) solid angle Ω . While in the case of 1D symmetry the angle ω can be chosen to be 180° , in models with the z axis as an axis of rotation symmetry, all planes within the angular region $(\theta_0 - \omega) \leq \theta \leq (\theta_0 + \omega)$ are combined, whereby θ_0 is the angle between the z axis and the normal vector of the observing plane. The corresponding (effective) solid angle Ω which is required to normalize the flux/intensity then amounts to $\Omega = 2\pi[\cos(\theta_0 - \omega) - \cos(\theta_0 + \omega)]$.
- (3) MC3D is prepared to take into account initial dust temperatures $T_g > 0$, such as in active accretion disks around young stellar objects. Therefore, the following modifications to the self-consistent RT process have to be applied:
 - *Iterative reemission*: The initial dust radiation field resulting from the initial dust temperature and dust density distribution (and dust grain optical properties) is added to the absorbed stellar radiation field in Eq. 15.
 - *Immediate concept*: The dust temperatures are set before the stellar RT is started. Thus, the absorbed stellar photons provide an additional increase of the dust grain temperature.
- (4) MC3D is equipped with a raytracer being optimized for the 1D and 2D models shown in Fig. 1. It allows derivation of images and the SED resulting from the dust reemission radiation. The basing assumption that scattering processes are negligible in the corresponding mid-infrared-millimeter wavelength range is very well fulfilled for most of the astrophysical applications targeted by MC3D.

Along rays, starting opposite to the observer's location (with respect to the model space), the contribution to the monochromatic luminosity is integrated taking into account extinction (see Fig. 6[A]). To take into account the emission/extinction of the smallest structures but also to guarantee a fast integration process, the step width of the numerical integration along a ray is adapted to the ESC grid, using a fraction of the ESC of the current integration point. The starting points of the rays are located in centrosymmetric rings (see Fig. 6[B]), whereby the inner/outer radii of these rings correspond to the radial subdivision of the model space into ESCs. The area within the inner radius of the models (where no subdivision of the model into ESCs is provided) is covered by rings with the inner/outer radius difference equal to that of the innermost ESC(s). Furthermore, the rings are subdivided in the azimuthal direction whereby the step width is chosen to achieve a similar resolution as in the radial direction. To increase the spatial resolution of the maps, each ring can be subdivided in a certain number of rings, and consequently smaller azimuthal subdivisions. To project the monochromatic luminosity determined in each of the resulting segments (each represented by a single ray) as shown in Fig. 6[B] and [C] on the matrix-like observing map, they

are subdivided in radial and azimuthal direction again.

6 Acknowledgements

I gratefully thank Olaf Fischer for his introduction into Monte Carlo radiative transfer – the numerical implementation of the basic scattering mechanism by spherical grains is mainly based on algorithms developed by him (Fischer (25)). I wish to thank both anonymous referees for their careful reading of the manuscript and their valuable comments and suggestions. This research was supported through the HST Grant GO 9160 through the NASA grant NAG5-11645, and through the DFG grant Ste 605/10 within the program “Physics of star formation”.

A Weighted mean optical parameters of dust grain mixtures

In case of non-self-consistent radiative transfer (RT) in a dust grain mixture, the numerical effort (ultimately, the CPU time and RAM requirement) may be substantially decreased by assuming weighted mean values of those parameters which describe the interaction of the electromagnetic field with the dust grains. The weight $w_j(a)$ which represents the contribution of a certain component of the dust grain mixture results from the abundance of the i th material of given dust grain number density (assuming n_D chemically different dust species) and the size distribution of the respective material:

$$\sum_{i=1}^{n_D} \int_{a_{\min}}^{a_{\max}} w_j(a) da = 1. \quad (\text{A.1})$$

The Stokes parameters as well as the extinction, absorption, and scattering cross section (C_{ext} , C_{abs} , C_{sca}) are additive. Therefore, the representative values in case of a dust grain mixture can be derived on the basis of their weighted contributions (see, e.g., Martin 1978, Šolc 1980):

$$\langle C_{\text{ext}} \rangle = \sum_{i=1}^{n_D} \int_{a_{\min}}^{a_{\max}} w_j(a) \cdot C_{\text{ext}_j}(a) da, \quad (\text{A.2})$$

$$\langle C_{\text{abs}} \rangle = \sum_{i=1}^{n_D} \int_{a_{\min}}^{a_{\max}} w_j(a) \cdot C_{\text{abs}_j}(a) da, \quad (\text{A.3})$$

$$\langle C_{\text{sca}} \rangle = \sum_{i=1}^{n_D} \int_{a_{\min}}^{a_{\max}} w_j(a) \cdot C_{\text{sca}_j}(a) da, \quad (\text{A.4})$$

and

$$\langle \hat{S} \rangle = \sum_{i=1}^{n_D} \int_{a_{\min}}^{a_{\max}} w_j(a) \cdot \hat{S}_j(a) da, \quad (\text{A.5})$$

where \hat{S} is the Müller matrix which is used to describe the modification of the photon's Stokes vector due to the interaction of a photon with the scattering/absorbing medium (dust grains; see Bickel & Bailey 1985, Bohren & Huffman 1983). For the albedo A follows:

$$\langle A \rangle = \frac{\sum_{j=1}^{n_D} \int_{a_{\min}}^{a_{\max}} w_j(a) \cdot C_{\text{ext}_j}(a) \cdot A_j(a) da}{\sum_{i=1}^{n_D} \int_{a_{\min}}^{a_{\max}} w_j(a) \cdot C_{\text{ext}_j}(a) da} = \frac{\langle C_{\text{sca}} \rangle}{\langle C_{\text{ext}} \rangle}. \quad (\text{A.6})$$

B Mean free path length

- (1) Decrease of the intensity of a plane wave due to extinction, described by Bouguer-Lambert's law

$$I_1 = I_0 \cdot e^{-\tau} \quad (\text{B.1})$$

(I_0 ... original intensity, I_1 ... intensity after passing a medium with the optical depth τ).

- (2) Let τ_{ext} be the optical depth due to dust extinction:

$$\tau = \tau_{\text{ext}} = \left[\sum_{j=1}^{n_D} C_{\text{ext}j} \cdot \rho_j \right] \cdot s \quad (\text{B.2})$$

($C_{\text{ext}j}$ is the wavelength-dependent extinction cross section of a single dust grain of the species number j , s is the geometric free path length, ρ_j is the number density of dust particles of that species)

assumption: $C_{\text{ext}j} \cdot \rho_j$ is constant along the geometrical distance s

- (3) Probability $f(\tau_{\text{ext}})d\tau_{\text{ext}}$ for a photon to pass a distance corresponding to the optical depth τ_{ext} :

$$\begin{aligned} f(\tau_{\text{ext}})d\tau_{\text{ext}} &= \frac{I_0 \cdot e^{-\tau_{\text{ext}}} \cdot d\tau_{\text{ext}}}{\int_0^\infty I_0 \cdot e^{-\tau_{\text{ext}}} d\tau_{\text{ext}}} \\ &= \frac{I_0 \cdot e^{-\tau_{\text{ext}}} \cdot d\tau_{\text{ext}}}{I_0} \\ &= e^{-\tau_{\text{ext}}} \cdot d\tau_{\text{ext}} \end{aligned} \quad (\text{B.3})$$

- (4) Resulting distribution of the optical depth $F(\tau_{\text{ext}})$:

$$F(\tau_{\text{ext}}) = \int_0^{\tau_{\text{ext}}} e^{-\tau'_{\text{ext}}} d\tau'_{\text{ext}} \quad (\text{B.4})$$

- (5) Determination of the free optical path length by substitution of $F(\tau_{\text{ext}})$ by a random number uniformly distributed in the interval $[0, 1]$:

$$\tau_{\text{ext}} = -\ln(1 - Z) . \quad (\text{B.5})$$

C Scattering matrix

The scattering Matrix (special Müller matrix) for the description of the modification of the Stokes vector due to the interaction of a weighted photon with

a spherical, homogeneous dust particle (Mie scattering) has the form

$$\hat{S}(\theta) = \begin{pmatrix} S_{11}(\theta) & S_{12}(\theta) & 0 & 0 \\ S_{12}(\theta) & S_{11}(\theta) & 0 & 0 \\ 0 & 0 & S_{33}(\theta) & S_{34}(\theta) \\ 0 & 0 & -S_{34}(\theta) & S_{33}(\theta) \end{pmatrix}, \quad (\text{C.1})$$

where

$$\begin{aligned} S_{11}(\theta) &= \frac{1}{2}(|S_1(\theta)|^2 + |S_2(\theta)|^2 + |S_3(\theta)|^2 + |S_4(\theta)|^2) \\ S_{12}(\theta) &= \frac{1}{2}(|S_2(\theta)|^2 - |S_1(\theta)|^2 + |S_4(\theta)|^2 - |S_3(\theta)|^2) \\ S_{33}(\theta) &= \text{Re}\{S_1(\theta)S_2^*(\theta) + S_3(\theta)S_4^*(\theta)\} \\ S_{34}(\theta) &= \text{Re}\{S_2(\theta)S_1^*(\theta) + S_4(\theta)S_3^*(\theta)\} \end{aligned} \quad (\text{C.2})$$

$$\begin{aligned} S_1 &= \sum_{n=1}^{\infty} \frac{2n+1}{n(n+1)} (a_n \pi_n + b_n \tau_n), \\ S_2 &= \sum_{n=1}^{\infty} \frac{2n+1}{n(n+1)} (a_n \tau_n + b_n \pi_n), \\ S_3 &= S_4 = 0 \end{aligned} \quad (\text{C.3})$$

$$a_n = \frac{\psi'_n(mx)\psi_n(x) - m\psi_n(mx)\psi'_n(x)}{\psi'_n(mx)\zeta_n(x) - m\psi_n(mx)\zeta'_n(x)}, \quad (\text{C.4})$$

$$b_n = \frac{m\psi'_n(mx)\psi_n(x) - \psi_n(mx)\psi'_n(x)}{m\psi'_n(mx)\zeta_n(x) - \psi_n(mx)\zeta'_n(x)}$$

$$\pi_n(\cos \theta) = \frac{1}{\sin \theta} P_n^1(\cos \theta), \quad (\text{C.5})$$

$$\tau_n(\cos \theta) = \frac{d}{d\theta} P_n^1(\cos \theta).$$

$P_n^1(\cos \theta)$ are associated Legendre functions, $\psi_n(x)$ und $\zeta_n(x)$ are Riccati-Bessel functions, m is the relative refraction index, and

$$x = \frac{2\pi}{\lambda} \cdot \|m_0\| \cdot a_K \quad (\text{C.6})$$

is the size parameter. The quantity m_0 is the refractive index of the surrounding medium³ λ is the wavelength of the infalling radiation and a_K is the dust particle radius (see Bohren & Huffman (19)).

The numerical formulation of the scattering mechanism for spherical, homogeneous particle is based on the algorithm presented by Fischer (25).

In case of Thomson scattering, the scattering matrix elements are wavelength-independent and can be written as

$$\begin{aligned} S_{11}(\theta) &= S_{22}(\theta) = (\cos^2(\theta) + 1)/2 \\ S_{12}(\theta) &= S_{21}(\theta) = (\cos^2(\theta) - 1)/2 \\ S_{33}(\theta) &= S_{44}(\theta) = \cos(\theta) \\ S_{13} &= S_{31} = S_{23} = S_{32} = 0 \\ S_{14} &= S_{24} = S_{34} = S_{43} = 0 \end{aligned} \tag{C.7}$$

(see Bohren & Huffman (19)).

The scattering cross section of an electron in this scattering regime is given by

$$\sigma_T = \frac{8\pi}{3} \cdot \left(\frac{e^2}{4\pi\epsilon_0 m_e c^2} \right)^2 \tag{C.8}$$

(e is the elementary charge, ϵ_0 is the dielectric constant of free space; see, e.g., Musiol et al. (26)).

D Reemission from ESCs

In the following the equations for the (random) determination of the reemission point within an ESC for the different models shown in Fig. 1 are given. According to the symmetry of the particular model, spherical (r, θ, ϕ) , cylindrical (r, ϕ, z) , or cartesian coordinates (x, y, z) are used.

Definition: Let ε be $\in \{x, y, z, r, \phi, \theta\}$. Then, ε_i and ε_{i+1} are the inner and outer boundary of the ESC along the coordinate ε , whereby $\varepsilon_{i+1} > \varepsilon_i$.

³ Since MC3D was developed to model astrophysical objects for which the surrounding medium can be assumed to be a perfect vacuum, $\|m_0\|=1$.

Model: 1D

$$\begin{array}{l} \text{Definition ranges:} \\ R_{\text{in}} \leq r \leq R_{\text{ou}} \\ 0^\circ \leq \theta \leq 180^\circ \\ 0^\circ \leq \phi < 360^\circ \end{array} \quad r = \left[Z_1(r_{i+1}^3 - r_i^3) + r_i^3 \right]^{\frac{1}{3}} \quad (\text{D.1})$$

$$\cos \theta = 1 - 2Z_2, \quad (\text{D.2})$$

$$\phi = 2\pi Z_3 \quad (\text{D.3})$$

Model: 2D(a)

$$\begin{array}{l} \text{Definition ranges:} \\ R_{\text{in}} \leq r \leq R_{\text{ou}} \\ \xi \leq \theta \leq 180^\circ - \xi \\ 0^\circ \leq \phi < 360^\circ \end{array} \quad r = \left[Z_1(r_{i+1}^3 - r_i^3) + r_i^3 \right]^{\frac{1}{3}} \quad (\text{D.4})$$

$$\cos \theta = (1 - 2Z_2) \sin \xi \quad (\text{D.5})$$

$$\phi = 2\pi Z_3 \quad (\text{D.6})$$

Model: 2D(b)

$$\begin{array}{l} \text{Definition ranges:} \\ R_{\text{in}} \leq r \leq R_{\text{ou}} \\ \xi \leq \theta \leq 180^\circ - \xi \\ 0^\circ \leq \phi < 360^\circ \end{array} \quad r = \left[Z_1(r_{i+1}^3 - r_i^3) + r_i^3 \right]^{\frac{1}{3}} \quad (\text{D.7})$$

$$\cos \theta = \cos \theta_{i+1} + Z_2(\cos \theta_i - \cos \theta_{i+1}) \quad (\text{D.8})$$

$$\phi = 2\pi Z_3 \quad (\text{D.9})$$

Model: 3D(a)

$$\begin{array}{l} \text{Definition ranges:} \\ 0 \leq x \leq l_c \\ 0 \leq y \leq l_c \\ 0 \leq z \leq l_c \end{array} \quad x = x_i + Z_1(x_{i+1} - x_i) \quad (\text{D.10})$$

$$y = y_i + Z_2(y_{i+1} - y_i) \quad (\text{D.11})$$

$$z = z_i + Z_3(z_{i+1} - z_i) \quad (\text{D.12})$$

Model: 3D(b)

$$\begin{array}{l} \text{Definition ranges:} \\ R_{\text{in}} \leq r \leq R_{\text{ou}} \\ 0^\circ \leq \theta \leq 180^\circ \\ 0^\circ \leq \phi < 360^\circ \end{array} \quad r = \left[Z_1(r_{i+1}^2 - r_i^2) + r_i^2 \right]^{\frac{1}{2}} \quad (\text{D.13})$$

$$\phi = \phi_i + Z_2(\phi_{i+1} - \phi_i) \quad (\text{D.14})$$

$$z = z_i + Z_3(z_{i+1} - z_i) \quad (\text{D.15})$$

Model 3D(c)

Definition ranges:

$$R_{\text{in}} \leq r \leq R_{\text{ou}}$$

$$0^\circ \leq \theta \leq 180^\circ$$

$$0^\circ \leq \phi < 360^\circ$$

$$r = \left[Z_1(r_{i+1}^3 - r_i^3) + r_i^3 \right]^{\frac{1}{3}} \quad (\text{D.16})$$

$$\cos \theta = \cos \theta_i + Z_2(\cos \theta_i - \cos \theta_{i+1}) \quad (\text{D.17})$$

$$\phi = \phi_i + Z_3(\phi_{i+1} - \phi_i) \quad (\text{D.18})$$

References

- [1] I. Pascucci, S. Wolf, J. Steinacker, et al., *A&A* (2002) in prep.
- [2] Wolf S., PhD thesis, Friedrich Schiller University, 2001
- [3] S. Wolf, Th. Henning, *Comp. Phys. Comm.* **132** (2000) 166.
- [4] S. Wolf, Th. Henning, B. Stecklum, *A&A* **439** (1999) 839.
- [5] J.E. Bjorkman, K. Wood, *ApJ* **554** (2001) 615.
- [6] L.B. Lucy, *A&A* **344** (1999) 282.
- [7] E.D. Cashwell, C.J. Everett, A practical manual on the Monte Carlo Method for random walk problems. Pergamon, New York, 1959
- [8] A. Witt, *ApJSS* **35** (1977) 1.
- [9] F. Ménard, PhD thesis, Université de Montréal, 1988
- [10] S. Wolf, F. Gueth, Th. Henning, W. Kley, *ApJ* **566** (2002) L97.
- [11] S. Wolf, O. Fischer, W. Pfau, *A&A* **340** (1998) 103.
- [12] S. Wolf, Th. Henning, B. Stecklum, *ASP Conf. Ser. , IAU Symposium 200 "The Formation of Binary Stars"* (2001) 295.
- [13] S. Wolf, Th. Henning, *A&A* **341** (1999) 675.
- [14] S. Wolf, N.V. Voshchinnikov, Th. Henning, *A&A* **385** (2002) 365.
- [15] S. Wolf, *A&A* **379** (2001) 607.
- [16] K. Wood, M.J. Wolff, J.E. Bjorkman, B. Whitney, *ApJ* **564** (2002) 887.
- [17] A.S. Cotera, B.A. Whitney, E. Young, *ApJ* **556** (2001) 958.
- [18] O. Fischer, Th. Henning, H.W. Yorke, *A&A* **308** (1996) 863.
- [19] C.F. Bohren, D.R. Huffman, Absorption and scattering of light by small particles. John Wiley & Sons, New York, 1983
- [20] S. Wolf, *ApJ*, 2002, in prep.
- [21] A.M. Sobolev, *Soviet Astronomy* **26** (1982) 366.
- [22] D.E. Knuth, in "Numerical Recipes (FORTRAN version)", eds. W.H. Press, B.P. Flannery, W.T. Vetterling, Cambridge University Press, Cambridge, 1989, p. 196-199
- [23] W.S. Bickel, W.M. Bailey, *Am. J. Phys.* **53** (5) (1985) 468.
- [24] O. Fischer, Th. Henning, H. Yorke, 1994, *A&A* **284**, 187.
- [25] O. Fischer, PhD thesis, Friedrich Schiller University, 1992
- [26] G. Musiol, J. Ranft, R. Reif, D. Seeliger, Kern- und Elementarteilchenphysik, VCH, Weinheim, New York, Cambridge, Basel, 1988

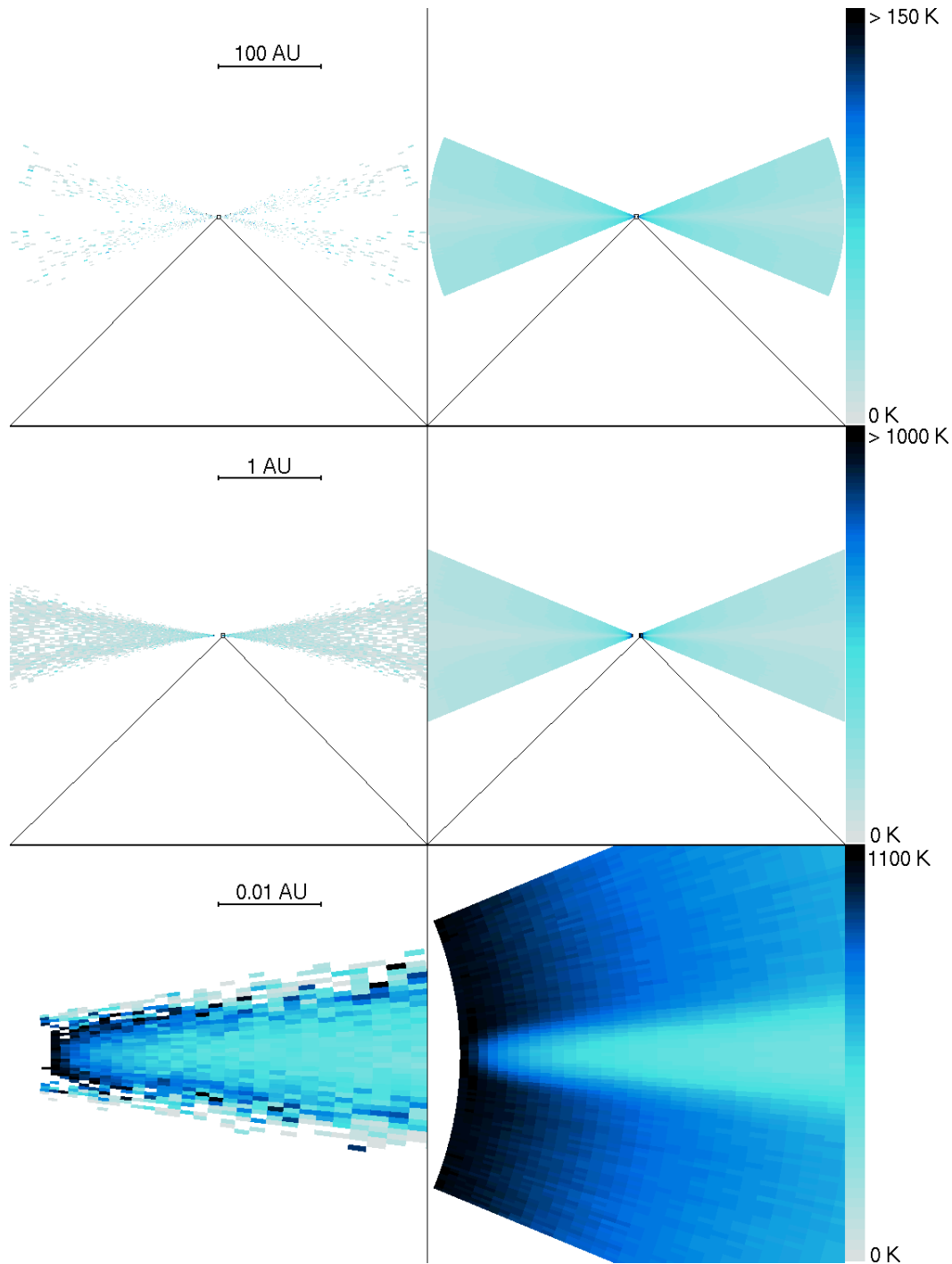


Fig. 4. Illustration of the high efficiency of the continuous absorption concept. While the temperature distribution shown in the left column was simulated without this concept, it was applied to achieve the results shown in the right column. Model: Density distribution of the model for the circumstellar disk around the T Tauri star HH 30 (from Cotera et al. 2001, Wood et al. 2002) but with only 10^{-2} of the mass assumed there. The disk is characterized by an optically thick midplane and an optically very thin “atmosphere” above the disk. The statistical noise of the temperature values is drastically smaller both in the regions of high and low optical depth if the continuous absorption concept is applied (the same number of 10^4 weighted photons was used in both simulations).

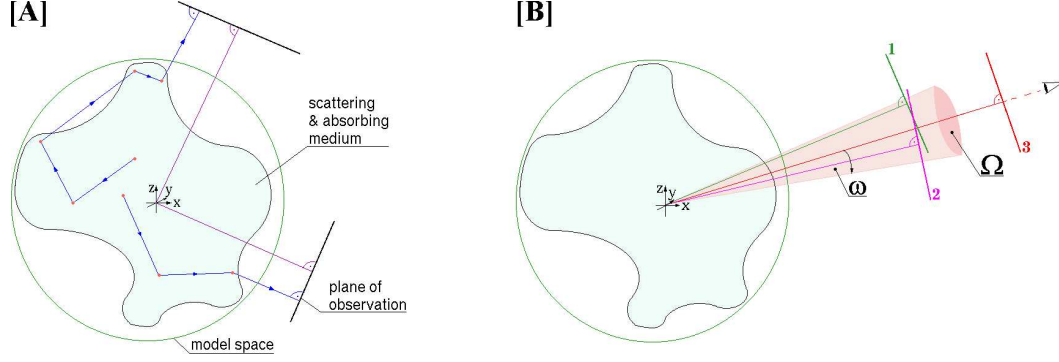


Fig. 5. [A] Random walk and projection of the weighted photons. [B] Definition of the solid angle Ω . The planes 1 and 2 are co-added with the infinite number of planes within the solid angle Ω .

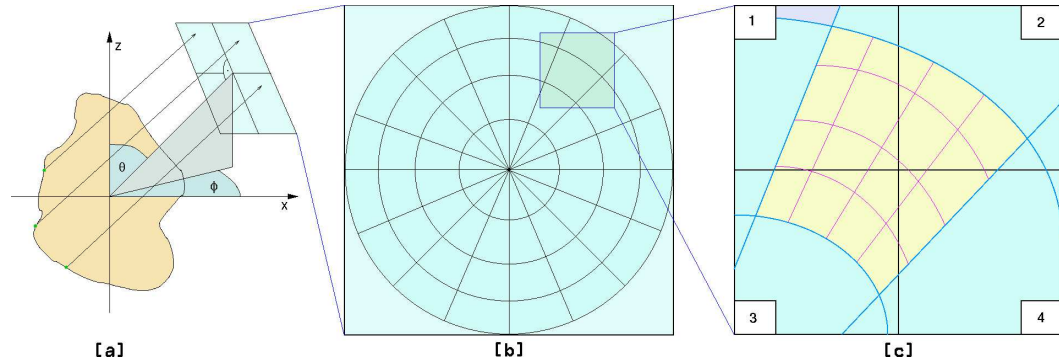


Fig. 6. Raytracer. [a] Projection of the monochromatic luminosity on the observing plane. [b] Configuration of the ray location on the observing plane. [c] Projection of each mapped region (represented by single ray) onto the matrix-like observing plane. The squares 1-4 symbolize single pixels.